Energy Management and Control of Photovoltaic and Storage Systems in Active Distribution Grids

Lysandros Tziovani, *Student Member, IEEE,* Lenos Hadjidemetriou, *Member, IEEE,* Panayiotis Kolios, *Member, IEEE,* Alessandro Astolfi, *Fellow, IEEE,* Elias Kyriakides, *Senior Member, IEEE,* and Stelios Timotheou, *Senior Member, IEEE*

Dedicated to the memory of Elias Kyriakides.

***Abstract*—The evolution of power distribution grids from passive to active systems creates reliability and efficiency challenges to the distribution system operators. In this paper, an energy management and control scheme for managing the operation of an active distribution grid with prosumers is proposed. A multi-objective optimization model to minimize (i) the prosumers electricity cost and (ii) the cost of the grid energy losses, while guaranteeing safe and reliable grid operation is formulated. This is done by determining the active and reactive power set-points of the photovoltaic and storage systems integrated in the grid buildings. The resulting optimization model is non-convex, thus a convex second-order cone program is developed by appropriately relaxing the non-convex constraints which yields optimal results in most operating conditions. The convexified model is further utilized to develop an algorithm that yields feasible solutions to the non-convex problem under any operating conditions. Moreover, a second novel algorithm to find the operating point that provides fairness between the prosumers and the grid costs is proposed. Simulation results demonstrate the effectiveness and superiority of the proposed scheme in managing an industrial distribution grid compared to a self-consumption approach.**

***Index Terms*—Convex relaxation, energy management, optimization, power flow constraints, reactive power support, smart distribution grids, voltage control.**

I. Introduction

THE integration of photovoltaic (PV) systems into the power system is expected to continue, with the aim to achieve full decarbonization of Europe's energy supply by 2050, according to the climate and energy strategy of the European Commission [1]. However, in cases in which massive PVs are integrated within a distribution grid, the stability and power quality of the grid is threatened mainly due to the uncontrollability of PV generation [2]. Energy storage systems (ESSs) can be used along with PV systems to compensate the negative effects of intermittent PV generation. ESSs constitute an emerging technology that enables optimized management of the energy produced by the PVs that can be utilized for peak shaving, load levelling, and reactive power support. Moreover, ESSs create new energy market opportunities for prosumers (users who consume, produce, store and sell energy), who are able to optimize their electricity management according to the electricity market price information [3]. However, since the prosumer actions can affect the safe operation of the low voltage (LV) distribution grid, the distribution system operator (DSO) and prosumers should be coordinated. This work aims to develop an energy management and control strategy to maximize the prosumers profits in active distribution grids with massive integration of PVs-ESSs, while maintaining the safe, reliable and cost-effective grid operation. In the proposed strategy, power flow constraints are integrated to ensure operating conditions within regulation limits, while reactive power support is provided by the PVs-ESSs.

Energy management and control strategies for voltage control in medium voltage (MV) distribution grids are presented in [4]-[5]. These strategies control the active and reactive power of the distributed generation to guarantee a safe and reliable grid operation. Similarly, strategies for voltage control in LV distribution grids determine the active and reactive power set-points of PV inverters in residential systems [6]-[7]. In addition to PV inverters, ESS inverters can also provide voltage control in LV and MV distribution grids by controlling their active and reactive power set-points [8]-[11]. These works do not consider the profit maximization of the prosumers at the building level in energy market environments. Multi-objective optimization schemes based on the weighted sum method for the system operation are presented in [4]-[7]; however, none of these works demonstrates the Pareto front to examine the trade-off of different objectives.

Energy management schemes at the building level to minimize the prosumer electricity cost under a time-based pricing are proposed in [12]-[15]. These do not consider reactive power support and the grid safety limits are ignored. Furthermore, energy management schemes at the grid level are presented in [16]-[20], where works in [16]-[17] and [20] optimize the electricity usage of the prosumers in LV distribution grids, while [18] and [19] minimize the operational cost of multiple microgrids which are connected to the MV distribution grid. Note that reactive power support is not provided by the PV-ESS systems in [16]-[17], [19] and the

This work was supported in part by the European Regional Development Fund and the Republic of Cyprus through the Research and Innovation Foundation under Project INTEGRATED/0916/0035 - EMPOWER; and in part by the European Union's Horizon 2020 research and innovation programme under grant agreement No 739551 (KIOS CoE - TEAMING) and from the Republic of Cyprus through the Deputy Ministry of Research, Innovation and Digital Policy.

L. Tziovani, L. Hadjidemetriou, P. Kolios and S. Timotheou are with the KIOS Research and Innovation Center of Excellence and the Department of Electrical and Computer Engineering, University of Cyprus, 1678 Nicosia, Cyprus (e-mail: {ltziov01, lhadji02, pkolios, stimo}@ucy.ac.cy).

E. Kyriakides, deceased, was with the KIOS Research and Innovation Center of Excellence and the Department of Electrical and Computer Engineering, University of Cyprus, 1678 Nicosia, Cyprus.

A. Astolfi is with the Department of Electrical and Electronic Engineering, Imperial College London, London SW7 2AZ, U.K., and with the Dipartimento di Ingegneria Civile e Ingegneria Informatica, Universita di Roma "Tor Vergata," 00133 Rome, Italy (e-mail: a.astolfi@imperial.ac.uk).

safe and reliable grid operation is not considered in [18], [20], since power flow constraints are ignored.

This work proposes a centralized energy management and control (CEMC) scheme to minimize (i) the prosumers electricity cost and (ii) the cost of the grid energy losses, while satisfying the safe and reliable grid operation. Towards this direction, a multi-objective optimization model to determine the active and reactive power set-points of the PV-ESS systems by minimizing the considered objectives is formulated. The safe grid operation is maintained through the integration of the power flow constraints in the optimization model, and reactive power support provided by PV-ESS inverters has a vital role in achieving reduced power losses and voltage regulation.

The resulting optimization model is non-convex, hence the underlying problem is challenging to solve; thus, convexification is used to transform the non-convex model to a convex second-order cone program (SOCP). Specifically, a convex relaxation of the power flow constraints is used, and a convex relaxation of the ESS power losses is proposed. Also, complementarity constraints that support different pricing schemes in the objective function are shown to hold in the considered problem and are eliminated from the formulation. The convex SOCP model allows computing optimal solutions under normal operating conditions; it can yield, however, infeasible solutions under "extreme" operating conditions. Therefore, an algorithm to provide a feasible solution when the relaxed SOCP model is non-exact is developed. In addition, a second novel algorithm to provide fairness between the prosumers and grid costs by minimizing the absolute difference between the gain losses of the two objectives[1] is proposed.

The effectiveness of the proposed CEMC scheme is compared to a self-consumption scheme, and simulation results validate the prosumers and grid cost-effective operation, as well as the grid reliability. Moreover, the performance of the proposed convex ESS model is compared with other ESS models, presented in the literature, in terms of energy losses and computational speed. In summary, this work has four main contributions.

1) A CEMC scheme for managing the PV-ESSs operation in smart distribution grids is introduced. The CEMC scheme minimizes both the prosumers electricity cost and the grid energy losses cost, while ensuring reliable grid operation by incorporating power flow constraints and reactive power support.
2) A convex multi-objective SOCP optimization model to solve fast and reliably the considered optimization problem by relaxing the non-convex constraints is formulated.
3) An algorithm to ensure feasibility of the relaxed SOCP model under all operating conditions is developed.
4) A second algorithm to find the operating point that minimizes the absolute difference between the objective gain losses is proposed.

The rest of the paper is organized as follows. Section II describes the system architecture, while Section III formulates the considered problem. The proposed solution methodology and the simulation results are presented in Sections IV and V, respectively. Conclusions are given in Section VI.

[1]We define the gain loss of an objective as the difference between the value of the particular objective, obtained when the two objectives are conflicting, and its minimum value, obtained when the other objective is not present in the formulation.

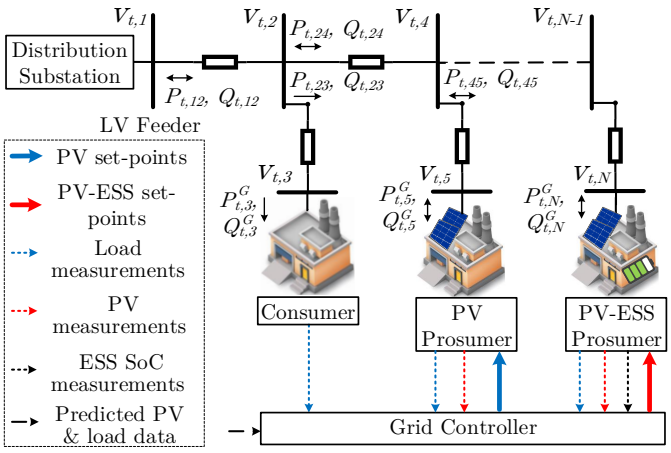

Fig. 1. Energy management and control of an industrial LV distribution grid.

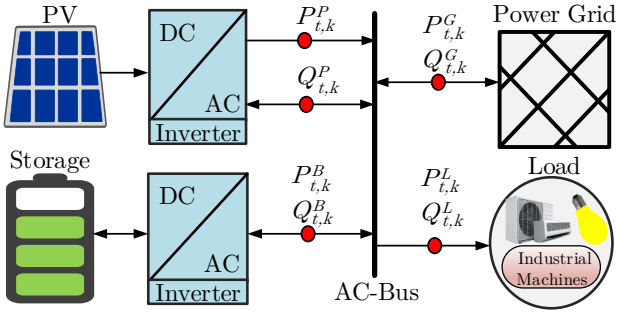

Fig. 2. The PV-ESS prosumer model.

II. System Architecture

We consider an industrial LV distribution grid that connects the industrial buildings (the prosumers) to an LV feeder through the distribution lines, as shown in Fig. 1. The power grid under consideration is radial, hence its graph is represented by a tree. Let the tree graph $\mathcal{G} = (\mathcal{N}, \mathcal{E})$ denote the power grid, where $\mathcal{N} = \{1, ..., N\}$ denote the set of grid buses and $\mathcal{E} = \{1, ..., E\}$ the set of grid lines that connect two buses. The LV feeder bus is the root of the tree. Let $\mathcal{B} \in \mathcal{N}$ denote the set of buses that are connected to the buildings; $\mathcal{M}_k \in \mathcal{N}$ the set of all buses that are children of bus k; $\mathcal{T} = \{1, ..., T\}$ the considered time horizon and ΔT the time-slot length in hours. For example, $\Delta T = 1/4$ denotes 15-minute time intervals. The active and reactive power flows of the grid line $(i, k) \in \mathcal{E}$ are given by $P_{t,ik}$ and $Q_{t,ik}$, $t \in \mathcal{T}$, with positive/negative values denoting direct/reverse power flows, respectively. Furthermore, the active and reactive power exchange between the building at bus $k \in \mathcal{B}$ and the grid are denoted by $P^G_{t,k}$ and $Q^G_{t,k}$, with positive/negative values denoting power consumption/generation of the buildings, respectively. The square of the voltage at each bus $n \in \mathcal{N}$ is denoted by v_n.

Three building models are considered in this work: (i) the *PV-ESS prosumer* consisting of an AC-coupled PV-ESS system, and a load; (ii) the *PV prosumer* comprising of a PV and a load; and (iii) the *consumer* which includes only a load.

Thus, $P^G_{t,k}$ and $Q^G_{t,k}$ are set according to the building model. The PV-ESS prosumer model is illustrated in Fig. 2. Note that $P^G_{t,k}$ and $Q^G_{t,k}$ can be adjusted by controlling the PV active and reactive power, $P^P_{t,k}$ and $Q^P_{t,k}$, and the ESS active and reactive power, $P^B_{t,k}$ and $Q^B_{t,k}$. The building load, $P^L_{t,k}$ and $Q^L_{t,k}$, must always be supplied by the power grid and/or the PV-ESS system, as indicated by the arrows in Fig. 2, denoting the power flow directions. Note that $P^B_{t,k}$ denotes discharging (charging resp.) power when $P^B_{t,k} \geq 0$ ($P^B_{t,k} < 0$), and $Q^P_{t,k}$ and $Q^B_{t,k}$ denote reactive power production (consumption) when they are positive (negative). Moreover, the PV prosumer and the consumer models are supported by setting $P^B_{t,k} = Q^B_{t,k} = 0$ and $P^B_{t,k} = Q^B_{t,k} = P^P_{t,k} = Q^P_{t,k} = 0$, respectively.

Under the proposed system structure, a grid-level controller (GC) is utilized to realize the CEMC scheme in a centralized manner, as described in Sections III and IV. As shown in Fig. 1, the GC regulates the power flows through the distribution grid, based on the predicted PV generation and load demand of prosumers, by setting the grid-buildings power exchange through the scheduling of PVs-ESSs power set-points. The prosumers execute the control signals sent by the GC regarding the PVs-ESSs active and reactive power set-points through their inverters. Due to the difference between predicted and actual PV generation, the PV inverters are allowed to operate at their maximum power point based on the actual available PV generation, except from the cases where PV power curtailments are applied by the GC. In these cases, the PV generation is limited to the PV active power set-point defined by the GC through the online reconfiguration of the inverter maximum power. The proposed control architecture is applied in a model predictive control (MPC) fashion, where at the end of every MPC control-step the GC defines the next PVs-ESSs power set-points. To achieve this, in every MPC control-step the GC uses the latest ESSs state-of-charge (SoC) measurements and updates the predicted PV and load data using the latest actual PV generation and load demand measurements of the buildings.

III. Problem Statement

This section contains the formulation of the optimization problem associated with the proposed CEMC scheme according to the system architecture described in Section II. In addition, the objective function and the constraints of the problem are presented.

A. Multi-objective Function

The considered CEMC scheme is a multi-objective optimization problem with two objective functions. The first objective describes the prosumers electricity cost in € by incorporating the cost of buying and selling energy

$$F_1(\mathbf{P}^b, \mathbf{P}^s) = \sum_{t\in\mathcal{T}} \sum_{k\in\mathcal{B}} (c^b_t P^b_{t,k} - c^s_t P^s_{t,k}) \Delta T, \tag{1a}$$

subject to the conditions

$$P^b_{t,k}, P^s_{t,k} \geq 0, \quad \forall t, k \in \mathcal{B}, \tag{1b}$$

$$P^b_{t,k} \perp P^s_{t,k}, \quad \forall t, k \in \mathcal{B}, \tag{1c}$$

where the variables $P^b_{t,k}$ and $P^s_{t,k}$ denote the buying and selling power of the building at bus k at time t in kW, respectively, and the parameters c^b_t and c^s_t denote the corresponding cost coefficients in €/kWh such that $c^b_t \geq c^s_t$. $\mathbf{P}^b$ and $\mathbf{P}^s$ are the vector-forms of the variables $P^b_{t,k}$ and $P^s_{t,k}$, for all $k \in \mathcal{B}$ and $t \in \mathcal{T}$, respectively. Note also that

$$P^G_{t,k} = P^b_{t,k} - P^s_{t,k}, \quad k \in \mathcal{B}, \forall t \in \mathcal{T}. \tag{2}$$

The variables $P^b_{t,k}$ and $P^s_{t,k}$ are used to support pricing schemes where the cost of buying and selling power can be different, while satisfying constraint (2). The non-convex complementarity constraint in (1c) restricts the ability to simultaneously buy and sell power to the grid [21]. Section IV-A indicates when the complementarity constraint can be eliminated.

The second objective quantifies the cost of energy losses at the grid lines in € and is given by

$$F_2(\mathbf{L}) = \sum_{t\in\mathcal{T}} \sum_{(i,k)\in\mathcal{E}} (r_{ik} l_{t,ik} c^b_t) \Delta T, \tag{3}$$

where $l_{t,ik}$ denotes the square of the current flow in line $(i,k) \in \mathcal{E}$ at time $t \in \mathcal{T}$, and r_{ik} denotes the line resistance. $\mathbf{L}$ is the vector-form of $l_{t,ik}$, for all $t \in \mathcal{T}$ and $(i,k) \in \mathcal{E}$.

The two objectives of the proposed CEMC scheme are transformed into an aggregated single objective by employing the widely used weighted sum method [4]-[7], [22]

$$F(w) = (1-w) F_1(\mathbf{P}^b, \mathbf{P}^s) + w F_2(\mathbf{L}), \tag{4}$$

where $w \in [0,1]$ is a weighting parameter that controls the tradeoff between the two objectives. Note that the two objectives are conflicting because the buildings-grid power exchange needs to be restrained in order to minimize the grid losses cost, which negatively affects the prosumer profits.

More sophisticated multi-objective optimization methods can also be employed for the considered biobjective problem, such as the adaptive weighted sum and normal boundary intersection (NBI) methods [23] - [25]. Using the NBI method a "knee" solution, which presents a good sense of "compromise" between the objectives, can be implicitly obtained without constructing the Pareto front [23]. In this work we explicitly find the tradeoff by minimizing the absolute difference between the gain losses of the two objectives.

B. Constraints

1) Power flow constraints: The power flow equations are conventionally formulated as sine and cosine functions of the voltage and current angles resulting in non-convex optimization problems. For radial grids, the branch-flow model [4], [26]-[27] can equivalently be used; this eliminates the voltage and current angles, yielding the equations

$$P_{t,ik} = r_{ik} l_{t,ik} + P^G_{t,k} + \sum_{m\in\mathcal{M}_k, m\neq i} P_{t,km}, \quad \forall t, (i,k) \in \mathcal{E}, \tag{5a}$$

$$Q_{t,ik} = x_{ik} l_{t,ik} + Q^G_{t,k} + \sum_{m\in\mathcal{M}_k, m\neq i} Q_{t,km}, \quad \forall t, (i,k) \in \mathcal{E}, \tag{5b}$$

$$v_{t,k} = v_{t,i} - 2(r_{ik} P_{t,ik} + x_{ik} Q_{t,ik}) + (r^2_{ik} + x^2_{ik}) l_{t,ik}, \quad \forall t, (i,k) \in \mathcal{E}, \tag{5c}$$

$$l_{t,ik} v_{t,i} = P_{t,ik}^2 + Q_{t,ik}^2, \quad \forall t, (i,k) \in \mathcal{E}. \tag{5d}$$

Eq. (5a) defines the active power flow through line (i,k) as the summation of the line power losses, the power exchange $P_{t,k}^G$ at bus k, if $k \in \mathcal{B}$, and the power flows through the connected lines. Similarly, the reactive power flow is defined in Eq. (5b), where x_{ik} is the line reactance. Eqs. (5c)-(5d) associate the power flows with the bus voltages and line currents. Lower/upper limits of the square of the voltage, $\underline{v}_j$ and $\overline{v}_j$, are set as

$$\underline{v}_j \leq v_{t,j} \leq \overline{v}_j, \quad \forall t, j \in \mathcal{N}. \tag{6}$$

For example, if the voltages must vary between -10% and +10% from their nominal value, then $\underline{v}_j = 0.9^2$ and $\overline{v}_j = 1.1^2$ p.u. Despite the elimination of the sine and cosine functions, the branch-flow model is still non-convex due to the presence of the constraint (5d).

2) Buildings active power management: The active power balance of a building, as illustrated in Fig. 2, is given by

$$P_{t,k}^P + P_{t,k}^B + P_{t,k}^G = P_{t,k}^L, \quad \forall t, k \in \mathcal{B}, \tag{7}$$

where $P_{t,k}^L$ denotes the building predicted active load demand in kW. PV power curtailments are applied when the PV power differs from the predicted PV generation, $\overline{P}_{t,k}^P$, and are set as

$$0 \leq P_{t,k}^P \leq \overline{P}_{t,k}^P, \quad \forall t, k \in \mathcal{B}. \tag{8}$$

The ESS SoC in kWh, $C_{t,k}^B$, is varied according to the discharging/charging power and the ESS power losses, $P_{t,k}^{loss}$, as expressed by

$$C_{t+1,k}^B = C_{t,k}^B + \Delta T(-P_{t,k}^B - P_{t,k}^{loss}), \quad \forall t, k \in \mathcal{B}. \tag{9}$$

The bounds of the ESS SoC, $\underline{C}_k^B$ and $\overline{C}_k^B$, and the discharging/charging power limitations, $\overline{P}_k^B$ and $\underline{P}_k^B$, are given by

$$\underline{C}_k^B \leq C_{t,k}^B \leq \overline{C}_k^B, \quad C_{0,k}^B = I_k^B, \quad \forall t, k \in \mathcal{B}, \tag{10a}$$

$$-\underline{P}_k^B \leq P_{t,k}^B \leq \overline{P}_k^B, \quad \forall t, k \in \mathcal{B}, \tag{10b}$$

where I_k^B denote the initial SoC value.

3) ESS power losses: Two linear power losses models, $P_{t,k}^{loss,c}$ and $P_{t,k}^{loss,d}$, are used to represent the ESS charging and discharging power losses, respectively, and formulated as

$$P_{t,k}^{loss,d} = e_k^d P_{t,k}^B, \quad P_{t,k}^{loss,c} = (-e_k^c) P_{t,k}^B \quad \forall t, k \in \mathcal{B}. \tag{11}$$

These models are dependent on the ESS charging/discharging power and the associated positive losses coefficients, e_k^c and e_k^d, respectively. Note that $e_k^d = 1/\eta_k^d - 1$ and $e_k^c = 1 - \eta_k^c$, where η_k^c and η_k^d are the charging/discharging (one-way) efficiency, respectively. $P_{t,k}^{loss,d}$ provides positive (negative) power losses when $P_{t,k}^B \geq 0$ ($P_{t,k}^B < 0$). In contrast, $P_{t,k}^{loss,c}$ provides positive (negative) power losses when $P_{t,k}^B < 0$ ($P_{t,k}^B \geq 0$). Thus, the ESS power losses are defined as the maximum of the two power losses models, that is

$$P_{t,k}^{loss} = \max(P_{t,k}^{loss,d}, P_{t,k}^{loss,c}), \quad \forall t, k \in \mathcal{B}. \tag{12}$$

Note that constraint (12) is non-convex, and logical constraints with binary variables are needed to represent it.

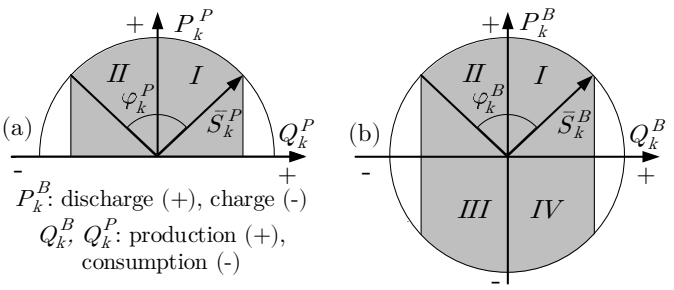

Fig. 3. The operating regions of (a) the PV and (b) the ESS inverters are given by the shaded area.

4) Buildings reactive power management: The reactive power balance in the building, as shown in Fig. 2, is set as

$$Q_{t,k}^G + Q_{t,k}^P + Q_{t,k}^B = Q_{t,k}^L, \quad \forall t, k \in \mathcal{B}, \tag{13}$$

where $Q_{t,k}^L$ denotes the building predicted reactive power demand in kVar. The PV-ESS inverter reactive power, $Q_{t,k}^P$ and $Q_{t,k}^B$ in kVar, is restricted by the inverter operation in active power, $P_{t,k}^P$ and $P_{t,k}^B$ in kW, and its maximum apparent power, $\overline{S}_k^P$ and $\overline{S}_k^B$ in kVA, according to the SOCP constraints:

$$(P_{t,k}^B)^2 + (Q_{t,k}^B)^2 \leq (\overline{S}_k^B)^2, \quad \forall t, k \in \mathcal{B}, \tag{14a}$$

$$(P_{t,k}^P)^2 + (Q_{t,k}^P)^2 \leq (\overline{S}_k^P)^2, \quad \forall t, k \in \mathcal{B}. \tag{14b}$$

The inverter limits in reactive power are given by

$$-\overline{S}_k^B \sin(\varphi_k^B) \leq Q_{t,k}^B \leq \overline{S}_k^B \sin(\varphi_k^B), \quad \forall t, k \in \mathcal{B}, \tag{15a}$$

$$-\overline{S}_k^P \sin(\varphi_k^P) \leq Q_{t,k}^P \leq \overline{S}_k^P \sin(\varphi_k^P), \quad \forall t, k \in \mathcal{B}, \tag{15b}$$

where the angle coefficients φ_k^P and φ_k^B are defined by the PV and ESS inverter power factor limits. Fig. 3 depicts the feasible operating regions of the inverters in terms of active and reactive power.

The considered MPC optimization problem that is solved by the GC at the end of every MPC control-step is summarized as

$$\mathbb{P}_{\mathrm{O}}(w): \begin{cases} \text{min Objective (4)} \\ \text{s.t.: Constraints (1b)} - \text{(1c)}, (2), (5a) - (15b), \end{cases}$$

with decision variables the active and reactive powers, $P_{t,k}^G$, $P_{t,k}^b$, $P_{t,k}^s$, $P_{t,k}^P$, $P_{t,k}^B$, $Q_{t,k}^G$, $Q_{t,k}^P$, $Q_{t,k}^B$, $\forall t \in \mathcal{T}$, $k \in \mathcal{B}$, the ESS power losses and SoC, $P_{t,k}^{loss}$, $P_{t,k}^{loss,d}$, $P_{t,k}^{loss,c}$, $C_{t,k}^B$, $\forall$ $t \in \mathcal{T}$, $k \in \mathcal{B}$, the power flows and the square of the line currents, $P_{t,ik}$, $Q_{t,ik}$, $l_{t,ik}$, $\forall$ $t \in \mathcal{T}$, $(i,k) \in \mathcal{E}$, as well as the square of the bus voltages, $v_{t,j}$, $\forall t \in \mathcal{T}, j \in \mathcal{N}$. Note that decision variables $P_{t,k}^P$, $P_{t,k}^B$, $Q_{t,k}^P$, $Q_{t,k}^B$ denote the active and reactive power set-points submitted to the PV-ESS inverters according to the system architecture of Section II. Problem $\mathbb{P}_{\mathrm{O}}(w)$ considers a single-phase system and can be used for balanced systems, using the single-phase equivalent. [4]. Problem $\mathbb{P}_{\mathrm{O}}(w)$ is non-convex, and hence challenging to solve due to the presence of the non-convex constraints (1c), (5d) and (12).

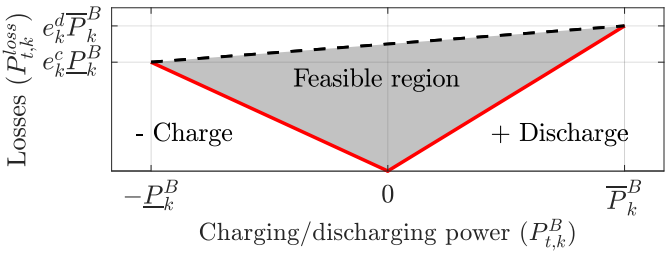

Fig. 4. ESS power losses convex relaxation. The losses are given as function of the charging/discharging power. The red solid lines show the losses when the relaxation is exact, and the dashed line provides upper bounds.

IV. Solution Methodology

In this section the non-convex problem $\mathbb{P}_O(w)$ is relaxed to a convex SOCP optimization problem and an algorithm to obtain feasible solutions under any operating condition is developed. Moreover, a second algorithm to define the best trade-off between the two conflicting objectives is proposed.

A. Convexifying Problem $\mathbb{P}_O(w)$

1) Relaxation of the power flow constraints: A convex SOCP relaxation of the non-convex constraint in (5d) is proposed in [4], [26]-[27], yielding

$$l_{t,ik} v_{t,i} \geq P^2_{t,ik} + Q^2_{t,ik}, \quad \forall t, (i,k) \in \mathcal{E}. \tag{16}$$

A sufficient condition for the relaxation exactness, where the equality is attained in Eq. (16), requires to have a strictly increasing objective function in the line currents ($l_{t,ik}$) [27]. Although the second objective, $F_2(\mathbf{L})$, is strictly increasing in $l_{t,ik}$, the presence of the first objective, $F_1(\mathbf{P}^b, \mathbf{P}^s)$, in objective (4), might affect the relaxation exactness.

2) Relaxation of the ESS power losses: The non-convex constraint in (12) is relaxed to the convex constraint:

$$P^{loss}_{t,k} \geq \max(P^{loss,d}_{t,k}, P^{loss,c}_{t,k}), \quad \forall t, k \in \mathcal{B}, \tag{17}$$

which can be represented by the affine constraints:

$$P^{loss}_{t,k} \geq e^d_k P^B_{t,k}, \quad \forall t, k \in \mathcal{B}, \tag{18a}$$

$$P^{loss}_{t,k} \geq -e^c_k P^B_{t,k}, \quad \forall t, k \in \mathcal{B}. \tag{18b}$$

Upper bounds on the maximum power losses, defined by the ESS maximum charging/discharging power and losses coefficients, are set as

$$P^{loss}_{t,k} \leq e^c_k \underline{P}^B_k + \alpha_k (P^B_{t,k} + \underline{P}^B_k), \quad \forall t, k \in \mathcal{B}, \tag{19a}$$

$$\alpha_k = (e^d_k \overline{P}^B_k - e^c_k \underline{P}^B_k)/(\overline{P}^B_k + \underline{P}^B_k), \quad \forall k \in \mathcal{B}. \tag{19b}$$

Fig. 4 shows the feasible region of the power losses defined by Eqs. (18a)-(19b). Note that the minimization of the function $F_1(\mathbf{P}^b, \mathbf{P}^s)$ is an incentive to satisfy the relaxation exactness, because higher power losses cause prosumers profit losses.

3) Elimination of complementarity constraints: According to (1c), the variables $P^b_{t,k}$ and $P^s_{t,k}$ should be complementary to each other. We now show that the structure of Problem $\mathbb{P}_O(w)$ automatically ensures that buying and selling power at the same time does not occur, hence the non-convex complementarity constraint (1c) can be eliminated.

Because $c^s_t \leq c^b_t$ we can write that $c^b_t = c^s_t + c$ for $c \geq 0$. It is also true that variables $P^b_{t,k}$ and $P^s_{t,k}$ appear as the difference $P^G_{t,k} = P^b_{t,k} - P^s_{t,k}$ in all constraints; they only appear separately in the first objective (1a) in which we have that:

$$\sum_{t\in\mathcal{T}} \sum_{k\in\mathcal{B}} (c^b_t P^b_{t,k} - c^s_t P^s_{t,k}) \Delta T = \sum_{t\in\mathcal{T}} \sum_{k\in\mathcal{B}} (c^s_t P^G_{t,k} + c P^b_{t,k}) \Delta T.$$

This implies that for a fixed positive or negative value of $P^G_{t,k}$ we aim to minimize $P^b_{t,k}$. Hence, when $P^G_{t,k} \geq 0$ and $P^G_{t,k} < 0$ the best objective is obtained for $P^G_{t,k} = P^b_{t,k}$, $P^s_{t,k} = 0$ and $P^G_{t,k} = -P^s_{t,k}$, $P^b_{t,k} = 0$, respectively. This argument shows that the complementarity constraint is automatically satisfied for Problem $\mathbb{P}_O(w)$.

Taking all convexifications into account yields:

$$\mathbb{P}_R(w): \begin{cases} \text{min Objective (4)} \\ \text{s.t.: Constraints (1b), (2), (5a)} - \text{(5c)}, \\ \text{(6)} - \text{(10b)}, \text{(13)} - \text{(15b)}, \text{(16)}, \text{(18a)} - \text{(19b)}. \end{cases}$$

Problem $\mathbb{P}_R(w)$ is a relaxed version of Problem $\mathbb{P}_O(w)$; hence, it provides a lower-bound solution to the latter. Due to the presence of (14a), (14b) and (16) the problem is a convex SOCP; hence, it can be fast and reliably solved for real-size distribution grids. Hereafter, the solution of Problem $\mathbb{P}_R(w)$ will be denoted with $\mathbf{x}_w$.

B. Obtaining Feasible Solutions to Problem $\mathbb{P}_O(w)$

The solution of Problem $\mathbb{P}_R(w)$ for a given w results in three cases with regards to the exactness of the non-convex constraints (5d) and (12) that need to be examined.

1) If both constraints (16) and (17) are tight (exact relaxation), the solution of Problem $\mathbb{P}_R(w)$ is optimal for $\mathbb{P}_O(w)$.
2) If constraint (16) is tight but (17) is not, the solution of Problem $\mathbb{P}_R(w)$ is feasible and provides an upper-bound for $\mathbb{P}_O(w)$.
3) If constraint (16) is loose (non-exact relaxation), the solution of Problem $\mathbb{P}_R(w)$ is infeasible for $\mathbb{P}_O(w)$.

Algorithm 1 summarizes the proposed procedure to find a feasible solution for Problem $\mathbb{P}_O(w)$ for a given w. Initially, Problem $\mathbb{P}_R(w)$ is solved (Line 2); the obtained solution is the optimal solution for Problem $\mathbb{P}_O(w)$ if it satisfies constraint (16) (Lines 3-4). Otherwise, the bisection method is employed to find the smallest weight $\hat{w} > w$ for which the solution of $\mathbb{P}_R(w)$ is tight for constraint (16) (Lines 5-13). The algorithm is based on the observation that higher values of w benefit the second objective, $F_2(\mathbf{L})$, causing to have a strictly increasing objective function in the line currents ($l_{t,ik}$), which is a sufficient condition for the tightness of the relaxed power flow constraint (16) [26]-[27]. The simulation results in Section V suggest that the solution of $P_R(w)$ is non-optimal only under

Algorithm 1 : Feasible Solution to Problem $\mathbb{P}_O(w)$

Input: w.
Solve $\mathbb{P}_R(w)$ to obtain $\mathbf{x}_w$.
if $\mathbb{P}_R(w)$ is feasible **then**
  Return $\mathbf{x}^* = \mathbf{x}_w$.
else
  Init. $w_l = w$, $w_u = 1$.
  while $(w_u - w_l) \geq \sigma$ **do**
    Set $w = (w_u + w_l)/2$;
    Solve $\mathbb{P}_R(w)$ to obtain $\mathbf{x}_w$;
    if $\mathbb{P}_R(w)$ is feasible **then**
      Set $w_u = w$, $\hat{\mathbf{x}} = \mathbf{x}_w$, $\hat{w} = w$.
    else
      Set $w_l = w$.
  Return $\hat{\mathbf{x}} = \mathbf{x}_w$ and $\hat{w}$

"extreme" operating conditions with high reverse-power flows in the grid. Even under these conditions, Algorithm 1 yields close-to-optimal results. In Algorithm 1, the bisection method is used to provide fast convergence to the operating point $\hat{w}$, providing a good quality feasible solution, $\hat{\mathbf{x}}$, for weight w. This method halves the searching space $(w_u - w_l)$ at each iteration, converging to $\hat{w}$ in $\log_2((1-w)/\sigma)$ iterations, where σ is the bisection tolerance.

C. Best Objective Trade-off Solution

Algorithm 1 solves Problem $\mathbb{P}_O(w)$ when w is known. This section proposes a novel algorithm, Algorithm 2, to provide a solution to Problem $\mathbb{P}_O$ when w is undefined. This is achieved by finding the operating point, w^*, for which Problem $\mathbb{P}_R(w^*)$ is feasible and the absolute difference of the gain losses of the two objectives is minimized.

Let $\mathbf{P}_w^b$, $\mathbf{P}_w^s$ and $\mathbf{L}_w$ denote the vectors $\mathbf{P}^b$, $\mathbf{P}^s$ and $\mathbf{L}$ derived from the solution of $\mathbb{P}_R(w)$, for $w \in [0,1]$. Then, $\underline{F}_1 = F_1(\mathbf{P}_0^b, \mathbf{P}_0^s)$ and $\underline{F}_2 = F_2(\mathbf{L}_1)$ denote the minimum values of the objectives in Eq. (4), $\forall\, w \in [0,1]$. The *prosumers gain loss*, G^p, and *grid gain loss*, G^g, are defined as

$$G^p(w) = F_1(\mathbf{P}_w^b, \mathbf{P}_w^s) - \underline{F}_1, \tag{20}$$
$$G^g(w) = F_2(\mathbf{L}_w) - \underline{F}_2. \tag{21}$$

G^p and G^g indicate the prosumers electricity cost and grid losses cost increments compared to the minimum values, respectively. Algorithm 2 aims to find the operating point w^* that minimizes $|G^p(w) - G^g(w)|$. Ideally, Algorithm 2 provides an operating point that equalizes the gain losses of the two objectives, i.e., $G^p(w^*) = G^g(w^*)$.

Note that $G^p(w) \in [0, G^p(1)]$ and $G^g(w) \in [0, G^g(0)]$, for $w \in [0,1]$. In addition, $G^p(w)$ is a monotonically increasing function and $G^g(w)$ is a monotonically decreasing function of w. Hence, it can be easily shown that $|G^p(w) - G^g(w)|$ is a unimodal function of w. For this reason, the bisection method is employed to find the minimal value of $|G^p(w) - G^g(w)|$ as shown in Algorithm 2. Note that if $w^* > \hat{w}$, where $\hat{w}$ is the value returned by Algorithm 1, then $G^p(w^*) = G^g(w^*)$, otherwise $w^* = \hat{w}$ and $G^p(w^*) > G^g(w^*)$. The reason for this is that Problem $\mathbb{P}_R(w)$ is feasible for $w \in [\hat{w}, 1]$, hence equalization of the gain losses occurs when $w^* > \hat{w}$.

Algorithm 2 : Trade-off Solution for Problem $\mathbb{P}_O$

Init. $w_l = 0$, $w_u = 1$.
Solve $\mathbb{P}_R(w_l)$ to obtain $\underline{F}_1$.
Solve $\mathbb{P}_R(w_u)$ to obtain $\underline{F}_2$.
while $(w_u - w_l \geq \sigma)$ **do**
  Set $w = (w_u + w_l)/2$.
  Solve $\mathbb{P}_R(w)$ to obtain $\mathbf{x}_w$, $G^p(w)$, $G^g(w)$.
  if $(G^p(w) > G^g(w))$ **and** $(\mathbb{P}_R(w)$ is feasible$)$ **then**
    Set $w_u = w$, $\mathbf{x}^* = \mathbf{x}_w$, $w^* = w$.
  else
    Set $w_l = w$.
Return $\mathbf{x}^*$, w^*, $G^p(w^*)$ and $G^g(w^*)$.

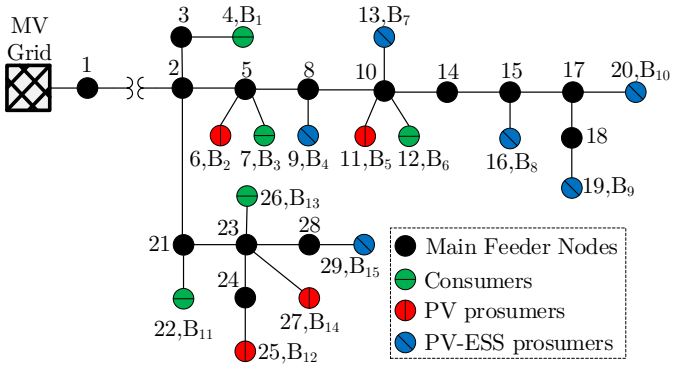

Fig. 5. Industrial LV distribution grid.

TABLE I
LINE IMPEDANCES

Line	R (Ω)	X (Ω)	Line	R (Ω)	X (Ω)	Line	R (Ω)	X (Ω)
2-3	0.0056	0.0294	10-12	0.0439	0.0280	2-21	0.0152	0.0801
3-4	0.0080	0.0051	10-13	0.0247	0.0104	21-22	0.0060	0.0060
2-5	0.0083	0.0435	10-14	0.0220	0.0545	21-23	0.0172	0.0906
5-6	0.0445	0.0283	14-15	0.0520	0.1291	23-24	0.0273	0.0678
5-7	0.0352	0.0224	15-16	0.0861	0.0548	24-25	0.0230	0.0146
5-8	0.0237	0.0588	15-17	0.0185	0.0460	23-26	0.0354	0.0225
8-9	0.0417	0.0266	17-18	0.0106	0.0263	23-27	0.0303	0.0193
8-10	0.0244	0.0607	18-19	0.0632	0.0403	23-28	0.0593	0.1472
10-11	0.0421	0.0268	17-20	0.0621	0.0395	28-29	0.0353	0.0225

V. SIMULATION RESULTS

To evaluate the performance of the proposed CEMC scheme, we have modified an industrial LV distribution grid of the Cyprus power system to consider a balanced system with 6 PV-ESS prosumers, 4 PV prosumers and 5 consumers, as shown in Figure 5. Towards this direction, we assume that (a) the load is uniformly distributed among the three phases, and (b) the three phases are decoupled [26]. The grid configuration and parameters have been provided by the Electricity Authority of Cyprus (Cyprus DSO). The positive-sequence impedances of the considered grid, where the line-to-line voltage is 400 volts, are given in Table I. The voltage limits are set to 0.9 and 1.1 p.u ($\underline{v}_j = 0.9^2$ and $\overline{v}_j = 1.1^2$ p.u), while the substation voltage is fixed at 1 p.u (node 2 of Fig. 5) [26].

The consumption building profiles have been synthesized

TABLE II
BUILDINGS DATA

	Load (Prof., kW)	PV (kW)	Storage (kWh, kW)		Load (Prof., kW)	PV (kW)	Storage (kWh, kW)
B1	LP2, 35	0	0, 0	**B9**	LP3, 20	20	20, 10
B2	LP3, 15	15	0, 0	**B10**	LP1, 22	22	25, 15
B3	LP1, 17	0	0, 0	**B11**	LP2, 30	0	0, 0
B4	LP2, 16	16	15, 7	**B12**	LP1, 21	21	0, 0
B5	LP1, 20	20	0, 0	**B13**	LP3, 18	0	0, 0
B6	LP2, 15	0	0, 0	**B14**	LP2, 20	20	0, 0
B7	LP3, 18	18	20, 10	**B15**	LP1, 25	25	25, 15
B8	LP2, 19	19	20, 10	-	-	-	-

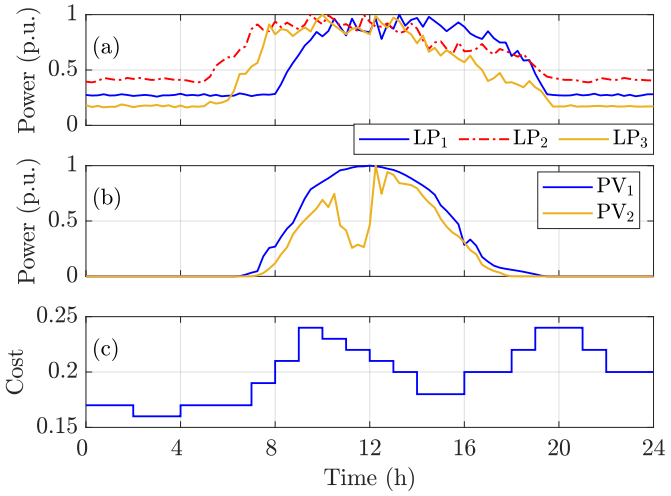

Fig. 6. (a) Load profiles. (b) PV profiles. (c) Day-ahead electricity pricing (Euro/kWh).

considering the normalized active power consumption of three industrial buildings, as shown in Fig. 6a. The power factor value of each building is set to 0.97. Similarly, the generation profile of the PV systems is synthesized based on two real-life normalized generation profiles, PV_1 for a sunny day and PV_2 for a partially cloudy day (Fig. 6b). The day ahead electricity price is also presented in Fig. 6c. Table II presents the load, PV and storage characteristics of the 15 buildings. For example, building B_4 uses load profile LP_2 with peak load demand, PV rated power, ESS capacity and ESS charging-discharging power equal to 16 kW, 16 kW, 15 kWh and 7 kW, respectively. Note that the power factor of the PV/ESS inverters is 0.9 ($\varphi_k^P = \varphi_k^B = 25.8°$), and the one-way efficiency of all ESSs is 96% ($\eta_k^c = 0.96$, $\eta_k^d = 0.96$). Thus, the losses coefficients in Eq. (11) are set as $e_k^c = 0.04$ and $e_k^d = 0.0416\ \forall k \in \mathcal{B}$. For reproducibility purposes, the input data that are used in this work are provided online in [28].

The proposed CEMC scheme is coded in Matlab, while Problem $\mathbb{P}_R$ is solved using the optimization solver Gurobi [29] on a personal computer with 8GB RAM and Intel Core-i5 3.2GHz. The horizon is set to one day with 15-minute time intervals, and the derived solution is applied in a rolling-horizon fashion. In Algorithms 1 and 2, we set $\sigma = 0.001$, resulting in a maximum of ten iterations.

The performance analysis and evaluation consider the trade-off between the objectives of the prosumers and the grid (Section V-A), compare the proposed CEMC scheme with a self-consumption scheme for a single operating scenario (Section V-B), and provide aggregate results on the performance of the two schemes under different normal operating conditions (Section V-C). Sections V-A to V-C assume perfect knowledge of PV generation and load demand, the predicted and actual PV generation and load demand are the same, while Section V-D investigates the performance of the proposed CEMC scheme considering PV uncertainty. Interestingly, both the power flow and the ESS convex relaxations are always exact in the aforementioned case studies; hence, further experimentation is undertaken under "extreme" operating conditions to understand when the convex relaxations are violated (Section V-E).

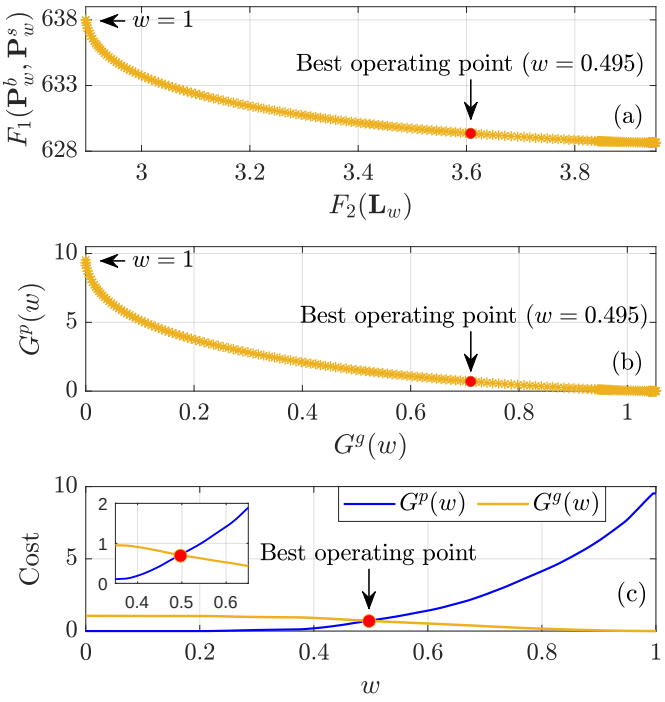

Fig. 7. Objectives trade-off: (a) Pareto front: Prosumers daily electricity cost and grid losses cost (€), (b) Prosumers and grid gain losses (€), and (c) Prosumers and grid gain losses as a function of w.

A. Objectives Trade-Off

The trade-off between the two objectives in (4) is presented in Fig. 7(a) by solving Problem $\mathbb{P}_O(w)$ using Algorithm 1 for $w \in \{0, 0.005, 0.01, ..., 1\}$, constructing the Pareto front of the two objectives. The figure indicates the Pareto optimal points, operating points, for each value of w where it is impossible to reduce the prosumers electricity cost, $F_1(\mathbf{P}_w^b, \mathbf{P}_w^s)$, without increasing the grid losses cost, $F_2(\mathbf{L}_w)$, and vice versa. Note that the solution of Problem $\mathbb{P}_R(w)$ (Step 2 of Algorithm 1) has generated tight solutions in all cases implying optimal results for $\mathbb{P}_O(w)$. Fig. 7(b) demonstrates the trade-off between the prosumers and grid gain losses, $G^p(w)$ and $G^g(w)$, while Fig. 7(c) illustrates the values of the prosumers and grid gain losses as a function of w. Interestingly, both Figs. 7(b) and 7(c) indicate that the maximum $G^p(w)$, observed for $w = 1$, is several times higher than the maximum $G^g(w)$, observed for $w = 0$. Note that the minimum values of the two gain losses

are observed for $w = 0$ and $w = 1$ ($G^p(0) = G^g(1) = 0$), where the corresponding objectives are given full priority. Figs. 7(b) and 7(c) also show that the best operating point, obtained from Algorithm 2, is at $w^* = 0.495$, where the prosumers gain loss, $G^p(w)$, and grid gain loss, $G^g(w)$, are equal, i.e., $G^p(w) = G^g(w)$. In this sense, this point provides fairness between the prosumers and the grid operator since they suffer from the same gain losses.

The execution time needed to derive all 201 operating points and hence construct the Pareto front is 378.7 sec, resulting in an average time of 1.88 sec to solve Problem $\mathbb{P}_R(w)$ for a single point. Nonetheless, in each MPC control-step of the CEMC scheme the GC does not need to construct the Pareto front; it only needs to find the best operating point according to Algorithm 2. The execution time of Algorithm 2 is 16.4 sec on average which is very small compared to the 15-minute control-step of the MPC.

B. Performance Evaluation

The performance of the proposed CEMC scheme is evaluated and compared with a self-consumption (SC) scheme in a single operating scenario using PV_2 when w is undefined. In the SC scheme, each PV-ESS prosumer operates in self-consumption mode, in which the ESS is charged when the building net load[2] is negative, and discharged otherwise; reactive power support is not provided.

The response of the grid operation based on the SC scheme and the proposed CEMC scheme are presented in Figs. 8 and 9, respectively. Figs. 8(a) and 9(a) depict the buildings-grid active power exchange for the 6 PV-ESS prosumers. As can be seen, the CEMC scheme maximizes the prosumers profits by (i) absorbing power to charge the ESSs when electricity prices are low (periods $2-4$ am and $2-4$ pm), and (ii) injecting power to the grid by discharging the ESSs when electricity prices are high (periods $9-10$ am and $7-9$ pm). The reactive power exchange for the 6 PV-ESS prosumers is shown in Figs. 8(b) and 9(b). In the SC scheme, the prosumers import reactive power to satisfy their load demand, while in the CEMC scheme they export reactive power to the grid through the PV-ESS inverters to provide reactive power support. Figs. 8(c) and 9(c) present the voltages of five critical nodes of the grid. As can be seen, the SC scheme experiences multiple voltage violations at buses 19 and 20, dropping below the safety limit of 0.9 p.u. In contrast, the CEMC scheme maintains the voltages close to their nominal values (1 p.u.) at all buses. Figs. 8(d) and 9(d) demonstrate the imported active and reactive power from the LV feeder. As expected from the reactive power support, the CEMC scheme dramatically reduces the reactive power compared to the SC scheme. Specifically, the CEMC scheme achieves 67% peak reduction and 79.3% total energy reduction. The peak active power is also reduced by 8.22%.

Table III presents the daily electricity cost of the six PV-ESS prosumers using the two schemes. The proposed CEMC scheme reduces the total daily electricity cost of the prosumers from €192.1 to €180.1 (6.2% reduction), the total grid losses

[2]The net load is defined as the difference between the load demand and the PV generation.

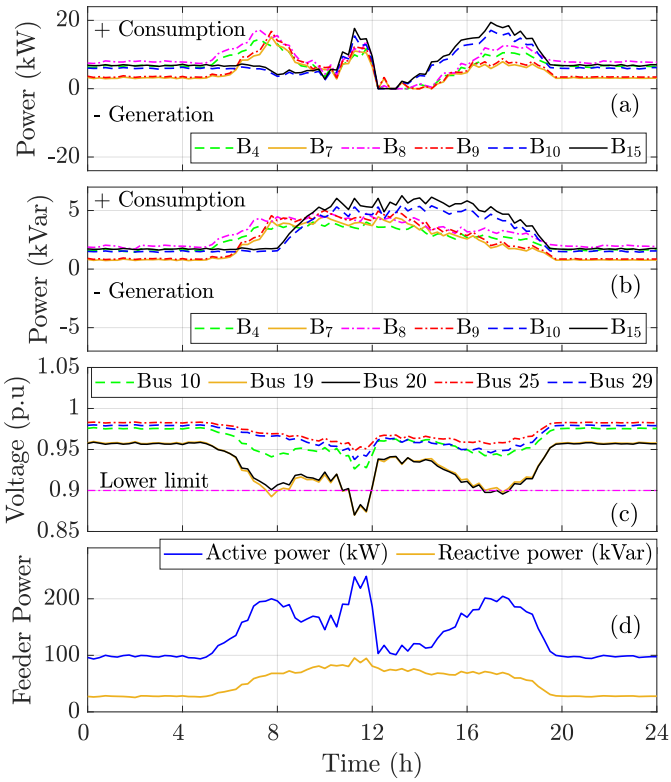

Fig. 8. Grid operation using the self-consumption (SC) scheme: (a) Active power exchange, (b) Reactive power exchange of the PV-ESS prosumers, (c) Voltages at five critical grid buses, (d) Feeder imported power.

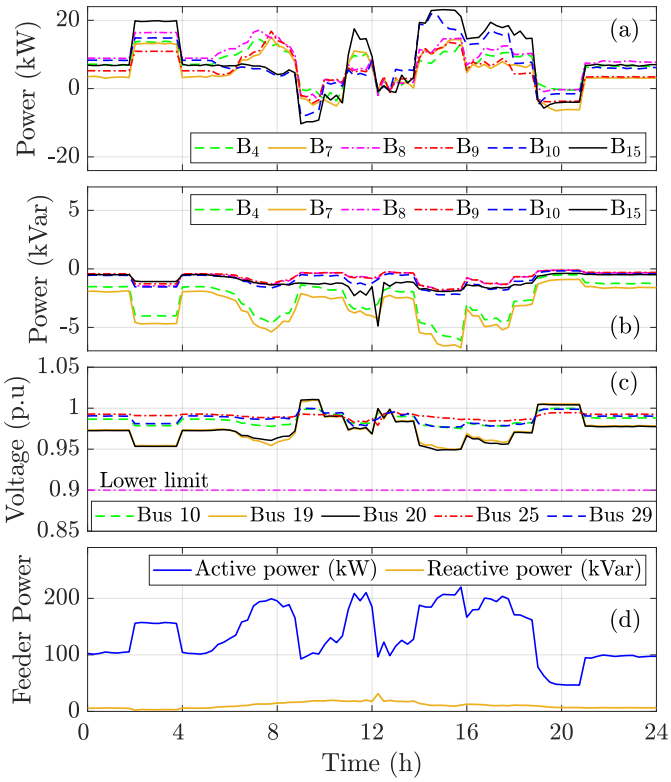

Fig. 9. Grid operation using the proposed CEMC scheme: (a) Active power exchange, (b) Reactive power exchange of the PV-ESS prosumers, (c) Voltages at five critical grid buses, (d) Feeder imported power.

TABLE III
PROSUMERS DAILY ELECTRICITY COST (€)

Buildings	B_4	B_7	B_8	B_9	B_{10}	B_{15}
SC scheme	32.87	23.03	39.03	25.59	33.51	38.08
CEMC scheme	31.39	21.01	37.13	23.75	31.30	35.49
Cost reduction	4.5%	8.8%	4.9%	7.2%	6.6%	6.8%

from 19.64 kWh to 19.03 kWh (3.1% reduction), and the grid losses cost from €3.98 to €3.61 (9.3% reduction), on average.

C. Aggregate Performance Evaluation

The performance of the proposed CEMC scheme is evaluated and compared with the SC scheme under different normal operating conditions when w is undefined. Twelve scenarios are carried out that involve combinations between (i) low, medium and high loads, (ii) sunny and cloudy days, and (iii) working and non-working days. The load values of Table II are considered to represent medium loads. The low (resp. high) loads are obtained by decreasing (resp. increasing) the medium loads by 30%. The load profiles of the working days are indicated in Figure 6; the base load of these profiles is considered as the load demand of the non-working days.

The results using the two schemes are demonstrated in Fig. 10, in box-plot form[3]. Fig. 10(a) shows the minimum and maximum bus voltages of the considered LV distribution grid. A 11.1% minimum voltage violation can be observed for the SC scheme; no violations are observed for the CEMC scheme. Fig. 10(b) illustrates that the CEMC scheme achieves considerable reduction of the maximum imported reactive power of the feeder. Specifically, the feeder maximum and median reactive power values are reduced by 65.1% and 65.5%, respectively.

Figs. 10(c) and 10(d) present the total electricity cost of the PV-ESS prosumers and the grid losses cost, respectively. As can be observed, the CEMC scheme achieves a 20.6% reduction of the median electricity cost compared to the SC scheme (€56.83 compared to €71.58), in exchange for a small increase in the grid losses cost (€2.55 compared to €1.81). This is because the SC scheme reduces the grid-buildings power exchange leading to low grid losses.

D. Performance Evaluation Considering PV Uncertainty

This section investigates the performance of the proposed CEMC scheme considering PV uncertainty for the scenario of Section V-B. Figure 11 depicts the predicted and actual PV generation for four different cases. PV_{A1} - PV_{A4} are real-life, normalized, partially-clouded, PV generation curves that are used as the actual, but unknown, PV generation profile of each considered case. Moreover, PV_P indicates the predicted PV generation (same with PV_2 in Fig. 6), used in

[3]The bottom and top of each box indicate the first and third quartiles (25% and 75%) of a ranked data set, while the horizontal line inside the box indicates the median value (second quartile). The horizontal lines outside the box indicate the lowest/highest datum still within 1.5 inter-quartile range of the lower/upper quartile; for normally distributed data this corresponds to approximately 0.35%/99.65%.

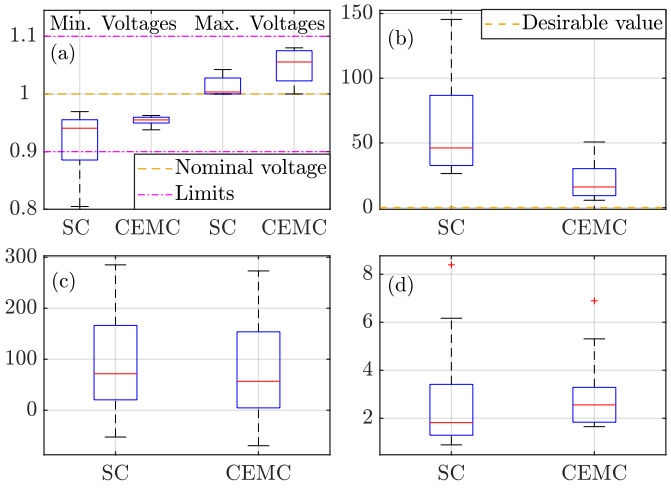

Fig. 10. Aggregate results of the SC and CEMC schemes: (a) Minimum and maximum bus voltages in p.u, (b) Maximum imported reactive power of the feeder in kVar, (c) Total daily cost of the PV-ESS prosumers in €, (d) Cost of the grid losses in €.

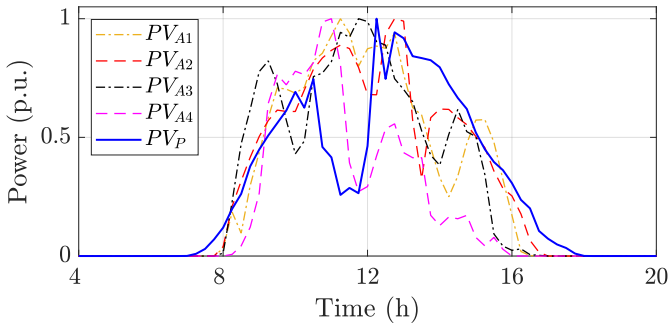

Fig. 11. PV curves used for performance evaluation under PV uncertainty. PV_{A1}, PV_{A2}, PV_{A3} and PV_{A4} are the actual PV curves in four different cases, while PV_P is the predicted PV curve in all cases.

all cases. Under the proposed control architecture, we examine the effectiveness of three CEMC variations:

- **CEMC**^{NU}: considers PV_P with no updates.
- **CEMC**^{U}: updates the PV_P curve for the examined MPC control-step t such that:
  $\text{PV}_P(t+1) \leftarrow 0.5(\text{PV}_A(t) + \text{PV}_P(t+1))$.
- **CEMC**^{P}: assumes perfect information such that:
  $\text{PV}_P(t) \leftarrow \text{PV}_A(t),\ \forall t$.

The three schemes are compared against the SC scheme. Note that although the CEMC^P scheme is unrealizable as it assumes knowledge of future information, it is used for comparison purposes as it provides the optimal performance.

Fig. 12(a) depicts the minimum voltages of the SC, CEMC^{NU}, CEMC^U and CEMC^P schemes in box-plot form for the four PV generation cases. Interestingly, voltage violations of the lower limit are presented in the SC scheme for all cases, while the CEMC^{NU} scheme generates significantly better results even with the large error between the predicted and actual PV generation. However, the CEMC^U scheme increases the minimum voltages, eliminating almost all violations, because the updating of the predicted PV generation in each MPC control-step corrects the reactive power support. As expected, the best results are provided under perfect knowl-

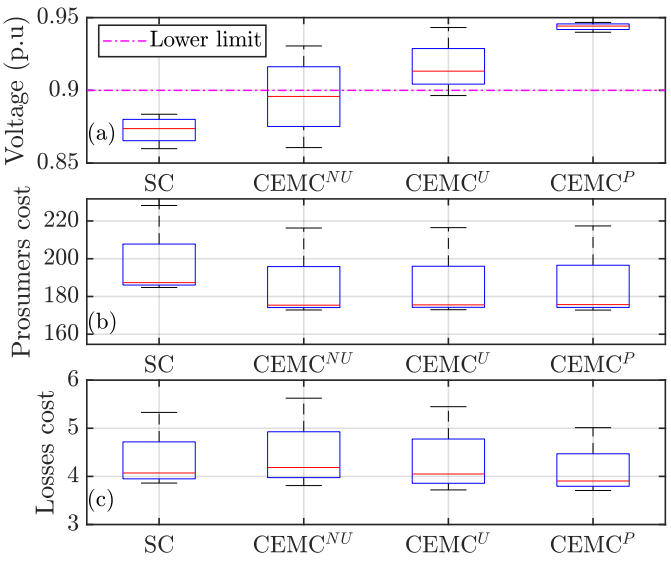

Fig. 12. Aggregate results of the SC, CEMC^{NU}, CEMC^{U} and CEMC^{P} schemes considering PV uncertainty: (a) Minimum voltage in p.u, (b) Total daily cost of the PV-ESS prosumers in €, (c) Cost of the grid losses in €.

edge of the PV generation (CEMC^{P}), avoiding all voltage violations. As depicted in Fig. 12(b), the CEMC^{NU}, CEMC^{U} and CEMC^{P} schemes reduce the total daily cost of the PV-ESS prosumers compared to the SC scheme, while the three CEMC schemes result to similar costs. As shown in Fig. 12(c), the CEMC^{NU} yields slightly higher grid losses costs compared to the SC scheme; however, the grid losses costs are reduced in the CEMC^{U} and CEMC^{P} schemes, where the latter generates the lowest grid losses costs. It is interesting to observe that the CEMC^{U} scheme handles well the PV generation uncertainty by avoiding almost all violations, despite using a very simple approach to update the predicted PV generation. Utilizing more sophisticated prediction schemes can yield even better performance.

E. Exactness of Convex Relaxations

An interesting observation that has emerged from the simulation results of Sections V-A to V-D is that the considered relaxations are always exact. Hence, in this section further experimentation is conducted to investigate the exactness of both the power flow and the ESS relaxations under the following "extreme" operating scenario: (i) PV generation: PV$_1$; (ii) Load demand: medium non-working day reduced by 80%; (iii) reduced upper limits of the voltages ($1.1-1.01$ p.u.); and (iv) no reactive power support ($Q^P_{t,k} = Q^B_{t,k} = 0,\ \forall t,k$). These scenario characteristics aim to increase the reverse power flow through the grid, cause the binding of the upper-bound voltage constraints, and apply PV curtailments, rather than reactive power support, for voltage control, in an effort to produce loose relaxation solutions. Perfect knowledge of PV generation and load demand is considered.

1) Exactness of the Power Flow Relaxation: Table IV presents (i) the operating point $\hat{w}$, (ii) the operating point w^*, (iii) the prosumers and grid gain losses, and (iv) the applied PV power curtailments, for different upper limit values of the voltage ($\overline{V} = \sqrt{\overline{v}_j}, \forall j \in \mathcal{N}$). As explained in Section IV-C,

TABLE IV
"EXTREME" OPERATING CONDITIONS - RESULTS

$\overline{V}$ (p.u)	$\hat{w}$	w*	G^p(w*)	G^g(w*)	PV curtailments
1.1	0.01	0.60	€2.77	€2.77	0 kWh
1.07	0.35	0.60	€2.77	€2.77	0 kWh
1.05	0.55	0.55	€3.92	€2.60	0 kWh
1.03	0.84	0.84	€30.3	€1.39	88.2 kWh
1.01	0.91	0.91	€89.1	€0.53	350 kWh

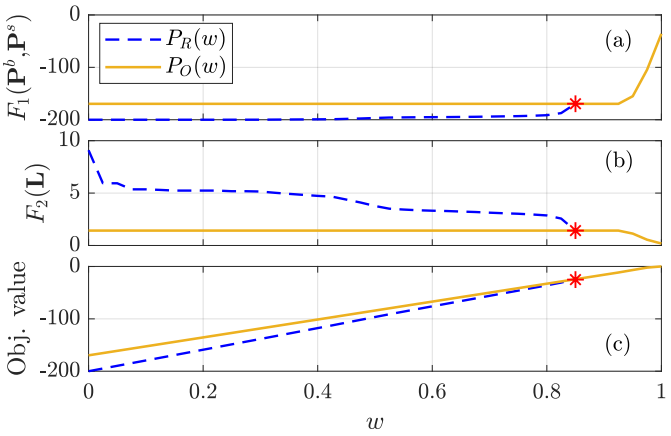

Fig. 13. Results for $\overline{V} = 1.03$: (a) prosumers electricity cost (€), (b) grid losses cost (€) and (c) objective function value.

the gain loss equalization, $G^p(w^*) = G^g(w^*)$, is attained when $w^* > \hat{w}$, which holds for $\overline{V} \geq 1.07$ p.u in this case. Note also that $G^p(w^*) > G^g(w^*)$, when $w^* = \hat{w}$, which is the case for $\overline{V} \leq 1.05$ p.u. Interestingly, the difference between $G^p(w^*)$ and $G^g(w^*)$ increases considerably as $\overline{V}$ drops below 1.05 p.u., due to the ESS set-points and the PV curtailments that are applied to maintain the voltages within bounds. Algorithm 2 ensures the exactness of the power flow relaxation.

The solution quality of $\mathbb{P}_O(w)$, obtained from Algorithm 1, is examined with respect to the lower bounds obtained from the solution of the relaxed problem $\mathbb{P}_R(w)$ for varying w. Figure 13 displays the prosumers electricity cost, $F_1(\mathbf{P}^b_w, \mathbf{P}^s_w)$, the grid losses cost, $F_2(\mathbf{L}_w)$, and the objective value, Eq. (4), derived from the solution of $\mathbb{P}_O(w)$ and $\mathbb{P}_R(w)$ when $\overline{V} = 1.03$. The graphs can be "separated" in two different regions. For $w \geq 0.84$, an exact relaxation is obtained from the solution of $\mathbb{P}_R(w)$ which is also optimal for $\mathbb{P}_O(w)$. As the solution of $\mathbb{P}_R(w)$ yields a non-exact relaxation for $w < 0.84$, Algorithm 1 is employed to obtain a feasible solution to $\mathbb{P}_O(w)$. To examine the quality of the solution to $\mathbb{P}_O(w)$, the optimality gap is considered

$$\text{Optimality Gap} = \frac{F_{\mathbb{P}_O}(w) - F_{\mathbb{P}_R}(w)}{F_{\mathbb{P}_R}(w)} \times 100\%, \qquad (22)$$

where $F_{\mathbb{P}_O}(w)$ and $F_{\mathbb{P}_R}(w)$ denote the objectives values derived from the solution of Problems $\mathbb{P}_O(w)$ and $\mathbb{P}_R(w)$. Interestingly, the maximum optimality gap is only 15.1% for $w = 0$ and is reduced as w increases. The reason is that increasing w makes the second objective of minimizing the grid losses cost more important, which causes the reduction of the power flows in the grid. This is achieved by utilizing the

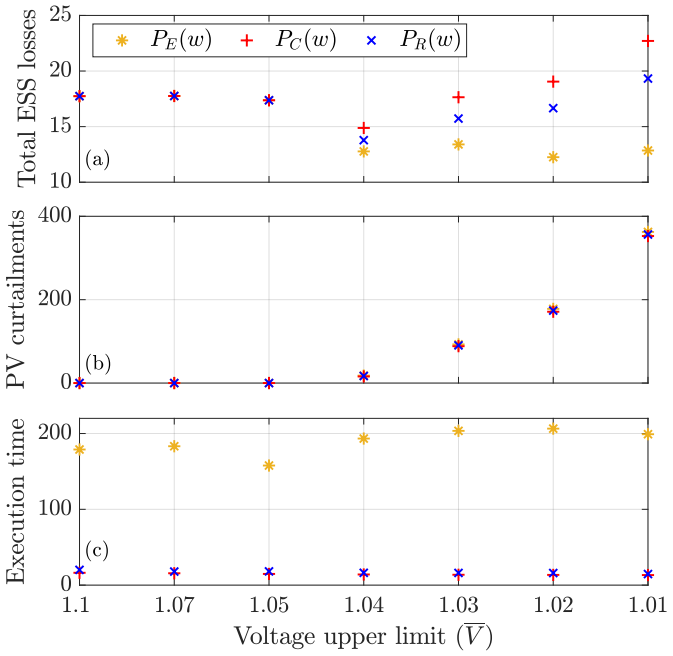

Fig. 14. Results for different ESS models: (a) total ESS energy losses (kWh), (b) PV curtailments (kWh) and (c) execution time of Algorithm 2 (sec).

ESSs and applying PV power curtailments, also contributing to the reduction of the voltage limits violation. The effect of these actions becomes more important as w increases, causing the gradual reduction of the optimality gap and eventually leading to the exactness of the power flow relaxation.

2) Exactness of the ESS Relaxation: The exactness of the proposed relaxed ESS model, constraints (18a) - (19b), is examined and compared with two ESS models employed in [30]-[32], presented in the Appendix. The first is the *exact non-convex ESS model* and the second is the relaxed version of the first model, the *relaxed convex ESS model*. To investigate the performance of these two ESS models in the CEMC scheme, we define the following problems:

- **Problem** $\mathbb{P}_E(w)$ is obtained by replacing the proposed ESS model, constraints (18a) - (19b), with the *exact non-convex ESS model*, Eqs. (A.1) - (A.4), in Problem $\mathbb{P}_R(w)$. Problem $\mathbb{P}_E(w)$ is a non-convex SOCP with complementarity constraints.
- **Problem** $\mathbb{P}_C(w)$ is obtained by replacing the proposed ESS model, constraints (18a) - (19b), with the *relaxed convex ESS model*, Eqs. (A.1) - (A.3), in Problem $\mathbb{P}_R(w)$. Problem $\mathbb{P}_C(w)$ is a convex SOCP.

Solutions to the two literature based ESS models are obtained by replacing Problem $\mathbb{P}_R(w)$ with $\mathbb{P}_E(w)$ and $\mathbb{P}_C(w)$ in Algorithm 2, respectively. The complementarity constraints (A.4) in Problem $\mathbb{P}_E(w)$ are handled by the optimization solver as type 1 special ordered set (SOS) constraints, where at most one variable in the specified list is allowed to take a non-zero value, indicated as SOS1$(P^d_{t,k}, P^c_{t,k})$, $\forall t, k \in \mathcal{B}$, [29].

Fig. 14(a) presents the total ESS energy losses[4] in kWh obtained by solving Problems $\mathbb{P}_R(w)$, $\mathbb{P}_E(w)$ and $\mathbb{P}_C(w)$, employing Algorithm 2, for different values of the voltage upper limit ($\overline{V}$). The results indicate that the two relaxed ESS models, associated with Problems $\mathbb{P}_R(w)$ and $\mathbb{P}_C(w)$, are exact for $\overline{V} \geq 1.05$ yielding the same losses with Problem $\mathbb{P}_E(w)$, while are non-exact for $\overline{V} \leq 1.04$. Interestingly, the proposed relaxed ESS model generates lower losses for $\overline{V} \leq 1.04$ compared to the relaxed literature-based ESS model. As can be seen in Fig. 14(b), the non-exactness of the ESS relaxations occurs only when PV power curtailments are applied. Note that power curtailments are presented for $\overline{V} \leq 1.04$ to satisfy the voltage upper limits. Consequently, extra ESS energy losses are introduced as an alternative power curtailment form by violating the ESS relaxation exactness, without affecting the solution feasibility. Fig. 14(c) demonstrates the execution time of Algorithm 2 in sec for Problems $\mathbb{P}_R(w)$, $\mathbb{P}_E(w)$ and $\mathbb{P}_C(w)$. As expected, the execution time of the non-convex SOCP problem (Problem $\mathbb{P}_E(w)$) is considerably higher (10-16 times higher) compared to the times of the convex SOCP problems ($\mathbb{P}_R(w)$ and $\mathbb{P}_C(w)$), which have similar execution times.

[4]The total ESS energy losses for Problems $\mathbb{P}_E(w)$ and $\mathbb{P}_C(w)$ are defined in the Appendix. For Problem $\mathbb{P}_R(w)$, the total ESS energy losses are calculated as $\sum_{t\in\mathcal{T}}\sum_{k\in\mathcal{B}}(P^{loss}_{t,k})\Delta T$.

VI. Conclusions

This work proposes an energy management and control scheme for managing the operation of an active distribution grid with prosumers. A non-convex multi-objective optimization model to minimize (i) the prosumers electricity cost and (ii) the grid energy losses cost, while maintaining the safe and reliable operation of the grid is formulated. The derived optimization problem is relaxed to a convex SOCP model and an algorithm to ensure feasibility under any operating condition is developed. Simulation results suggest that the relaxed optimization problem yields optimal solutions under normal operating conditions, while the associated algorithm yields close-to-optimal results under "extreme" operating conditions, for which the relaxations are not exact. Moreover, a novel algorithm to find an operating point that provides fairness between the prosumers and the grid costs is proposed. Simulation results indicate the effectiveness and superiority of the proposed scheme in comparison with a self-consumption approach, even under PV generation uncertainty. Future work will explore energy management and control schemes for unbalanced distribution grids.

Appendix A: Literature-Based ESS Models

The *exact non-convex ESS model* presented in [30]-[32] is expressed as

$$C^B_{t+1,k} = C^B_{t,k} + \Delta T(-\frac{1}{\eta^d_k}P^d_{t,k} + \eta^c_k P^c_{t,k}), \quad \forall t, k \in \mathcal{B}, \quad \text{(A.1)}$$

$$\underline{C}^B_k \leq C^B_{t,k} \leq \overline{C}^B_k, \quad C^B_{0,k} = I^B_k, \quad \forall t, k \in \mathcal{B}, \quad \text{(A.2)}$$

$$0 \leq P^d_{t,k} \leq \overline{P}^B_k, \quad 0 \leq P^c_{t,k} \leq \underline{P}^B_k, \quad \forall t, k \in \mathcal{B}, \quad \text{(A.3)}$$

$$P^d_{t,k} \perp P^c_{t,k} \quad \forall t, k \in \mathcal{B}, \quad \text{(A.4)}$$

where variables $P^d_{t,k}$ and $P^c_{t,k}$ denote the discharging and charging power, respectively. The non-convex complementarity constraint (A.4) restricts the simultaneous charging and discharging power.

The non-convex ESS model, Eqs. (A.1) - (A.4), is relaxed to the convex ESS model in [30]-[32] by removing the complementarity constraint (A.4). The *relaxed convex ESS model* is exact when simultaneous charging and discharging power does not occur. Note that when the two ESS models are used in Problem $\mathbb{P}_R(w)$ instead of the proposed ESS model, then variables $P^B_{t,k}$ must be replaced by $P^B_{t,k} = P^d_{t,k} - P^c_{t,k}$ in the formulation. Under the two literature-based ESS models, the power losses are given

$$\hat{P}^L_{t,k} = e^d_k P^d_{t,k} + e^c_k P^c_{t,k} \quad \forall t, k \in \mathcal{B}. \tag{A.5}$$

The total ESS energy losses are calculated as $\sum_{t\in\mathcal{T}} \sum_{k\in\mathcal{B}} (\hat{P}^L_{t,k}) \Delta T$.

REFERENCES

[1] European Commission, "2050 Climate and Energy Strategy,"

[2] J. Dong et al., "Distribution voltage control: current status and future trends," in *Proc. IEEE PEDG*, Charlotte, NC, 2018, pp. 1-7.

[3] L. Park et al., "Prosumer energy management considering contract with consumers under progressive pricing policy," *IEEE Access*, vol. 8, pp. 115789-115799, 2020.

[4] C. Feng, Z. Li, M. Shahidehpour, F. Wen, W. Liu and X. Wang, "Decentralized short-term voltage control in active power distribution systems," *IEEE Trans. Smart Grid*, vol. 9, no. 5, pp. 4566-4576, 2018.

[5] Q. Nguyen et al., "Exact optimal power dispatch in unbalanced distribution systems with high PV penetration," *IEEE Trans. Power Systems*, vol. 34, no. 1, pp. 718-728, Jan. 2019.

[6] E. Dall'Anese, S. V. Dhople and G. B. Giannakis, "Optimal dispatch of photovoltaic inverters in residential distribution systems," *IEEE Trans. Sustain. Energy*, vol. 5, no. 2, pp. 487-497, Apr. 2014.

[7] X. Su, M. A. S. Masoum and P. J. Wolfs, "Optimal PV inverter reactive power control and real power curtailment to improve performance of unbalanced four-wire LV distribution networks," *IEEE Trans. Sustain. Energy*, vol. 5, no. 3, pp. 967-977, Jul. 2014.

[8] D. Ranamuka, K. M. Muttaqi and D. Sutanto, "Flexible AC Power Flow Control in Distribution Systems by Coordinated Control of Distributed Solar-PV and Battery Energy Storage Units," *IEEE Trans. Sustain. Energy*, vol. 11, no. 4, pp. 2054-2062, Oct. 2020.

[9] J. Tant, F. Geth, D. Six, P. Tant and J. Driesen, "Multiobjective battery storage to improve PV integration in residential distribution grids," *IEEE Trans. Sustain. Energy*, vol. 4, no. 1, pp. 182-191, Jan. 2013.

[10] D. Zarrilli et al., "Energy storage operation for voltage control in distribution networks: A receding horizon approach," *IEEE Trans. Control Systems Technology*, vol. 26, no. 2, pp. 599-609, Mar. 2018.

[11] P. Fortenbacher, J. L. Mathieu and G. Andersson, "Modeling and optimal operation of distributed battery storage in low voltage grids," *IEEE Trans. Power Systems*, vol. 32, no. 6, pp. 4340-4350, Nov. 2017.

[12] L. Tziovani et al., "Grid friendly operation of a PV-storage system with profit maximization and reliability enhancement," in *Proc. IEEE SEST*, Porto, Portugal, 2019, pp. 1-6.

[13] P. M. van de Ven et al., "Optimal control of end-user energy storage," *IEEE Trans. Smart Grid*, vol. 4, no. 2, pp. 789-797, Jun. 2013.

[14] L. Tziovani et al., "Energy scheduling in non-residential buildings integrating battery storage and renewable solutions," in *Proc. IEEE ENERGYCON*, Limassol, Cyprus, 2018, pp. 1-6.

[15] S. Kim, J. Kim, K. Cho and G. Byeon, "Optimal operation control for multiple BESSs of a large-scale customer under time-based pricing," *IEEE Trans. Power Systems*, vol. 33, no. 1, pp. 803-816, Jan. 2018.

[16] J. Hu, Y. Li and H. Zhou, "Energy management strategy for a society of prosumers under the IOT environment considering the network constraints," *IEEE Access*, vol. 7, pp. 57760-57768, May 2019.

[17] P. Zhuang et al., "Hierarchical and decentralized stochastic energy management for smart distribution systems with high BESS penetration," *IEEE Trans. Smart Grid*, vol. 10, no. 6, pp. 6516-6527, Nov. 2019.

[18] P. Tian et al., "A hierarchical energy management system based on hierarchical optimization for microgrid community economic operation," *IEEE Trans. Smart Grid*, vol. 7, no. 5, pp. 2230-2241, Sept. 2016.

[19] H. Gao, J. Liu, L. Wang and Z. Wei, "Decentralized energy management for networked microgrids in future distribution systems," *IEEE Trans. Power Systems*, vol. 33, no. 4, pp. 3599-3610, Jul. 2018.

[20] M. Rastegar, M. Fotuhi-Firuzabad and M. Moeini-Aghtai, "Developing a two-level framework for residential energy management," *IEEE Trans. Smart Grid*, vol. 9, no. 3, pp. 1707-1717, May 2018.

[21] P. Olivella-Rosell et al., "Centralised and Distributed Optimization for Aggregated Flexibility Services Provision," *IEEE Trans. Smart Grid*, vol. 11, no. 4, pp. 3257-3269, July 2020.

[22] R. Timothy Marler and J. S. Arora, "The weighted sum method for multiobjective optimization: New insights," *Structural and Multidisciplinary Optimization*, vol. 41, pp. 853–862, Jun. 2010.

[23] C. Zhang et al., "Multi-Objective Adaptive Robust Voltage/VAR Control for High-PV Penetrated Distribution Networks," *IEEE Trans. Smart Grid*, vol. 11, no. 6, pp. 5288-5300, Nov. 2020.

[24] C. Roman and W. Rosehart, "Evenly distributed pareto points in multiobjective optimal power flow," *IEEE Trans. Power Systems*, vol. 21, no. 2, pp. 1011-1012, May 2006.

[25] Y. Fu et al., "Multiobjective Stochastic Economic Dispatch With Variable Wind Generation Using Scenario-Based Decomposition and Asynchronous Block Iteration," *IEEE Trans. Sustainable Energy*, vol. 7, no. 1, pp. 139-149, Jan. 2016.

[26] L. Gan, N. Li, U. Topcu and S. H. Low, "Exact Convex Relaxation of Optimal Power Flow in Radial Networks," in *IEEE Trans. on Automatic Control*, vol. 60, no. 1, pp. 72-87, Jan. 2015.

[27] M. Farivar and S. H. Low, "Branch flow model: Relaxations and convexification-Part I," *IEEE Trans. Power Systems*, vol 28, no.3, pp. 2554-2564, Aug. 2013.

[28] L. Tziovani, L. Hadjidemetriou, P. Kolios, A. Astolfi, E. Kyriakides and S. Timotheou. Data set for study "Energy Management and Control of Photovoltaic and Storage Systems in Active Distribution Grids," 2021. [Online]. Available: "http://doi.org/10.5281/zenodo.4767415"

[29] Gurobi Optimization, LLC, "Gurobi Optimizer Reference Manual," 2020. [Online]. Available: "http://www.gurobi.com".

[30] Z. Li, Q. Guo, H. Sun and J. Wang, "Sufficient Conditions for Exact Relaxation of Complementarity Constraints for Storage-Concerned Economic Dispatch," in *IEEE Trans. on Power Systems*, vol. 31, no. 2, pp. 1653-1654, March 2016.

[31] P. Yang and A. Nehorai, "Joint Optimization of Hybrid Energy Storage and Generation Capacity With Renewable Energy," in *IEEE Trans. on Smart Grid*, vol. 5, no. 4, pp. 1566-1574, July 2014.

[32] C. Shao et al., "Cooperative Dispatch of Wind Generation and Electric Vehicles With Battery Storage Capacity Constraints in SCUC," in *IEEE Trans. on Smart Grid*, vol. 5, no. 5, pp. 2219-2226, Sept. 2014.

Lysandros Tziovani (Student Member, IEEE) received the B.Sc. and M.Sc. degrees in electrical engineering from the University of Cyprus, Nicosia, Cyprus, in 2015 and 2017, respectively, where he is currently pursuing the Ph.D. degree with the Department of Electrical and Computer Engineering and a Researcher with KIOS Research and Innovation Center of Excellence. His research interests lie in the area of electric power systems, power system operation, and optimization.

Lenos Hadjidemetriou (Member, IEEE) received the Diploma in Electrical and Computer Engineering in 2010 from the National Technical University of Athens, Athens, Greece, and his Ph.D. degree in Electrical Engineering in 2016 from the University of Cyprus. He is currently a Research Lecturer at the KIOS Research and Innovation Center of Excellence, University of Cyprus, Cyprus. His research interests include renewable energy systems, energy storage systems, control of power electronics, ancillary services, smart grids and microgrids. Dr. Hadjidemetriou has published more than 75 papers in scientific journals and international conference proceedings. He has extensive experience on managing research projects in the area of smart grids and he has developed 3 advanced research laboratories in the University of Cyprus premises. Dr. Hadjidemetriou is a member of the Cyprus Technical Chamber. He volunteered as a reviewer to several IEEE transactions and conferences and received the best paper award in the power quality session at IEEE IECON13.

Panayiotis Kolios (Member, IEEE) received the B.Eng. and Ph.D. degrees in telecommunications engineering from King's College London, in 2008 and 2011, respectively. He is currently a Research Assistant Professor with the KIOS Research and Innovation Center of Excellence, University of Cyprus. His interests focus on both basic and applied research on networked intelligent systems. Some examples of such systems include intelligent transportation systems, autonomous unmanned aerial systems, and the plethora of cyber-physical systems that arise within the Internet of Things. Particular emphasis is given to emergency response aspects in which faults and attacks could cause disruptions that need to be effectively handled. He is an Active Member of IEEE, contributing to a number of technical and professional activities within the association.

Alessandro Astolfi (Fellow, IEEE) was born in Rome, Italy, in 1967. He graduated in electrical engineering from the University of Rome in 1991. In 1992 he joined ETH-Zurich where he obtained a M.Sc. in Information Theory in 1995 and the Ph.D. degree with Medal of Honor in 1995 with a thesis on discontinuous stabilization of nonholonomic systems. In 1996 he was awarded a Ph.D. from the University of Rome La Sapienza for his work on nonlinear robust control. Since 1996 he has been with the Electrical and Electronic Engineering Department of Imperial College London, London (UK), where he is currently Professor of Nonlinear Control Theory and Head of the Control and Power Group. From 1998 to 2003 he was also an Associate Professor at the Dept. of Electronics and Information of the Politecnico of Milano. Since 2005 he has also been a Professor at Dipartimento di Ingegneria Civile e Ingegneria Informatica, University of Rome Tor Vergata. He has been/is visiting lecturer in Nonlinear Control in several universities, including ETHZurich (1995-1996); Terza University of Rome (1996); Rice University, Houston (1999); Kepler University, Linz (2000); SUPELEC, Paris (2001), Northeastern University (2013), University of Cyprus (2018–), Southeast University (2019–).

His research interests are focused on mathematical control theory and control applications, with special emphasis for the problems of discontinuous stabilization, robust and adaptive control, observer design and model reduction. He is the author of more than 170 journal papers, of 30 book chapters and of over 400 papers in refereed conference proceedings. He is the author (with D. Karagiannis and R. Ortega) of the monograph "Nonlinear and Adaptive Control with Applications" (Springer-Verlag).

He is the recipient of the IEEE CSS A. Ruberti Young Researcher Prize (2007), the IEEE RAS Googol Best New Application Paper Award (2009), the IEEE CSS George S. Axelby Outstanding Paper Award (2012), the Automatica Best Paper Award (2017). He is a "Distinguished Member" of the IEEE CSS, IEEE Fellow, IFAC Fellow, IET Fellow, and member of the Academia Europaea. He served as Associate Editor for Automatica, Systems and Control Letters, the IEEE Trans. on Automatic Control, the International Journal of Control, the European Journal of Control and the Journal of the Franklin Institute; as Area Editor for the Int. J. of Adaptive Control and Signal Processing; as Senior Editor for the IEEE Trans. on Automatic Control; and as Editor-in-Chief for the European Journal of Control. He is currently Editor-in-Chief of the IEEE Trans. on Automatic Control. He served as Chair of the IEEE CSS Conference Editorial Board (2010-2017) and in the IPC of several international conferences. He was/is a Member of the IEEE Fellow Committee (2016/2019-2022).

Elias Kyriakides (Senior Member, IEEE) received the B.Sc. degree from the Illinois Institute of Technology, Chicago, IL, USA, in 2000, and the M.Sc. and Ph.D. degrees from Arizona State University, Tempe, AZ, USA, in 2001 and 2003, respectively, all in electrical engineering. He was an Associate Professor with the Department of Electrical and Computer Engineering, University of Cyprus, Nicosia, Cyprus, and a founding Member of the KIOS Research and Innovation Center of Excellence, University of Cyprus. His research interests included wide area monitoring and control of power systems, the optimization of power system operation techniques, and the integration of renewable energy sources. He served as the Action Chair of the ESF-COST Action IC0806 "Intelligent Monitoring, Control, and Security of Critical Infrastructure Systems" from 2009 to 2013. He was an Associate Editor of the IEEE Systems Journal and an Editor of the IEEE Transactions on Sustainable Energy.

Stelios Timotheou (Senior Member, IEEE) is an Assistant Professor at the Department of Electrical and Computer Engineering and a faculty member at the KIOS Research and Innovation Center of Excellence of the University of Cyprus. He holds a Dipl.-Ing. in Electrical and Computer Engineering (Summa Cum Laude, 2005) from the National Technical University of Athens, an MSc in Communications and Signal Processing (Distinction, 2006) and a PhD in Intelligent Systems and Networks (2010), both from the Department of Electrical and Electronic Engineering of Imperial College London. In previous appointments, he was a Research Associate at KIOS, a Visiting Lecturer at the Department of Electrical and Computer Engineering of the University of Cyprus, and a Postdoctoral Researcher at the Computer Laboratory of the University of Cambridge. His research focuses on monitoring, control and optimization of critical infrastructure systems, with emphasis on intelligent transportation systems, communication systems and power systems. He is the recipient of the 2017 Cyprus Young Researcher in Physical Sciences & Engineering Award, by the Cyprus Research Promotion Foundation.